Analyzing postprandial metabolomics data using multiway models: A simulation study

Lu Li[1], Shi Yan[1], Barbara M. Bakker[2], Huub Hoefsloot[3], Bo Chawes[4], David Horner[4], Morten A. Rasmussen[4,5], Age K. Smilde[1,3], Evrim Acar[1*]

1 Department of Data Science and Knowledge Discovery, Simula Metropolitan Center for Digital Engineering, Oslo, Norway
2 Laboratory of Pediatrics, Section Systems Medicine and Metabolic Signalling, Center for Liver, Digestive and Metabolic Disease, University of Groningen, University Medical Center Groningen, Groningen, the Netherlands
3 Swammerdam Institute for Life Sciences, University of Amsterdam, Amsterdam, The Netherlands
4 Copenhagen Prospective Studies on Asthma in Childhood (COPSAC), Herlev and Gentofte Hospital, University of Copenhagen, Copenhagen, Denmark
5 Department of Food Science, University of Copenhagen, Copenhagen, Denmark

* evrim@simula.no

Abstract

Analysis of time-resolved postprandial metabolomics data can improve the understanding of metabolic mechanisms, potentially revealing biomarkers for early-diagnosis of metabolic diseases and advancing precision nutrition and medicine. Postprandial metabolomics measurements at several time points from multiple subjects can be arranged as a *subjects* by *metabolites* by *time points* array. Traditional analysis methods are limited in revealing subject groups, related metabolites, and temporal patterns simultaneously from such three-way data. In this paper, we introduce an unsupervised multiway analysis approach based on the CANDECOMP/PARAFAC (CP) model for improved analysis of postprandial metabolomics data guided by a simulation study. Because of the lack of ground truth in real data, we generate simulated data using a comprehensive human metabolic model. This allows us to assess the performance of CP models in terms of revealing subject groups and underlying metabolic processes. We study three analysis approaches: analysis of *fasting-state* data using Principal Component Analysis, *T0-corrected* data (i.e., data corrected by subtracting *fasting-state* data) using a CP model and *full-dynamic* (i.e., full postprandial) data using CP. Through extensive simulations, we demonstrate that CP models capture meaningful and stable patterns from simulated meal challenge data, revealing underlying mechanisms and differences between diseased vs. healthy groups. Our simulations also show that it is crucial to analyze both *fasting-state* and *T0-corrected* data for understanding metabolic differences among subject groups. Depending on the nature of the subject group structure, the best group separation may be achieved by CP models of *T0-corrected* or *full-dynamic* data. Furthermore, we show that the proposed approach reveals differences between subject groups (according to body mass index) in terms of their response to a real meal challenge test. This study introduces an improved analysis approach for postprandial metabolomics data while also shedding light on the debate about correcting baseline values in longitudinal data analysis.

Author summary

Postprandial metabolomics data can mirror the ability of the human body to cope with a meal challenge. Analysis of such data can reveal differences among subject groups, discover biomarkers related to (early-onset) disease and holds the promise to guide personalized nutrition. However, traditional analysis methods are limited in terms of revealing the underlying patterns from such time-resolved data which is inherently a multiway array: a *subjects* by *metabolites* by *time points* array. In this paper, we introduce an unsupervised approach based on multiway data analysis for postprandial metabolomics data, and assess its performance using simulated data based on a comprehensive human metabolic model. We demonstrate that the overall picture of metabolic differences among subject groups (e.g., healthy vs. diseased) and the underlying metabolic processes can be captured through the analysis of *fasting-state* data and multiway analysis of the *dynamic* data. We show the promise of the proposed approach through real postprandial metabolomics data analysis and discuss the patterns revealing metabolic differences among subject groups (according to body mass index (BMI)) in terms of their response to a meal challenge test.

Introduction

Postprandial metabolomics data (also referred to as meal challenge test data) includes the metabolic transition from the fasting to the fed state. Analysis of such data can reveal the underlying biological processes and improve the understanding of metabolic mechanisms [1, 2]. Examples include the study of a high-fat meal response for over one thousand subjects, which revealed subclass patterns in lipoprotein metabolism [3]. Analysis of postprandial metabolomics data also holds the promise to reveal new biomarkers especially for cardiometabolic diseases [4, 5]. In addition to detecting biomarkers and advancing prediagnosis, studying the postprandial state has proven useful in designing personalized nutrition [6]. Because of the high variability between individuals in terms of their post-meal glucose and triglyceride levels, personalized dietary interventions can be considered to lower individual post-meal glucose, thus may help decrease the risk of diseases such as prediabetes [6, 7].

There are various methods available for analyzing meal challenge test data. These are mainly supervised approaches, i.e., assuming that the group information (e.g., labels such as healthy and diseased) is known and incorporated into the analysis. In the aforementioned and other related work, univariate analyses are the most used tools for analyzing postprandial metabolism, e.g., the repeated measures analysis of variance (ANOVA) method is used to test group differences [3, 5]; a linear mixed model (LMM), which adds the random effect in the analysis, is used to explore the time and group interaction effect [8]. Univariate methods are simple and powerful in terms of studying group differences; however, such analyses are performed per metabolite, thus unable to reveal the relation between metabolites. Since metabolites are interlinked via pathways and hold dependent or independent relations with other metabolites, multivariate analyses are promising in capturing the underlying patterns in the data [4, 9]. Supervised multivariate methods used to analyze metabolomics data from challenge tests are often methods combining ANOVA or LMM with principal component analysis (PCA). Such methods include ANOVA-Simultaneous Component Analysis (ASCA) [10], ANOVA-PCA [11], ANOVA-Partial Least Squares (PLS) [12], and their extensions [13, 14]. While these methods are suitable for time-resolved data, they rely on a priori known group information.

When the goal is exploratory analysis to reveal unknown stratification of subjects such as subgroups among healthy or diseased subjects, the workhorse data analysis

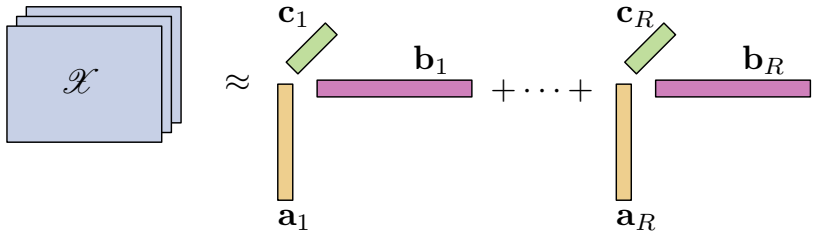

Fig 1. An R-component CP model of a three-way array with modes: *subjects*, *metabolites*, and *time*. Vectors $\mathbf{a}_r$, $\mathbf{b}_r$ and $\mathbf{c}_r$ correspond to the patterns in the *subjects*, *metabolites*, and *time* modes.

approaches are unsupervised methods based on PCA and clustering [9]. However, these approaches cannot exploit the three-way structure of postprandial metabolomics data. They rely on either measurements at one time point or data summaries such as clusters of time profiles obtained using data averaged across subjects [2, 15]. An effective way to preserve the multiway nature of the data and extract the underlying patterns is to use tensor factorizations [16–18], which are extensions of matrix factorizations such as PCA to multiway arrays (higher-order data sets).

In this paper, we arrange time-resolved metabolomics data as a three-way array with modes: *subjects*, *metabolites*, and *time*, and use the CANDECOMP/PARAFAC (CP) [19, 20] tensor model to reveal the underlying patterns. The CP model summarizes the three-way array as a sum of a small number of factor triplets as in Fig 1. Among various tensor factorization methods, we use the CP model because of its uniqueness properties [16, 21], which facilitate interpretability of the extracted factors. The CP model has previously been mentioned as a promising analysis tool for meal challenge test data [4, 9], but no analysis results have been presented for the three-way data arranged as in Fig 1. Recently, the effectiveness of the CP model in terms of analyzing other types of longitudinal data has been studied, e.g., using gut microbiome data from infants studying microbial changes and how those relate to the birth mode [22], urine metabolomics data from newborns exploring the use of the CP model for compositional data [23] and simulated dynamic metabolomics data relying on small-scale metabolic pathway models [24]. Unlike previous studies, we provide a comprehensive study of the CP model for analyzing time-resolved metabolomics data, in particular, focusing on the human metabolism in response to a meal challenge test and studying metabolic changes from a baseline state to dynamic states.

In the literature, analysis of *full-dynamic* data (i.e., full postprandial data without baseline correction) as well as *T0-corrected* data (i.e., the data corrected by subtracting the *fasting* state, similar to the method of analysis of changes [25]) have been considered [1, 2, 5, 26, 27]. Note that the *full-dynamic* data has information from the *fasting* as well as the *T0-corrected* (*pure-dynamic*) state. Understanding metabolic differences between these two states can help understand the metabolic mechanisms for postprandial metabolomics data. Therefore, we consider the analysis of *fasting-state* data, *T0-corrected* data and *full-dynamic data* to provide a complete picture of the underlying metabolic processes.

In order to assess the performance of analysis approaches in terms of revealing the underlying patterns in the data, we generate simulated postprandial metabolomics data with known ground-truth information. To mimic the evolution of metabolite concentrations during a meal challenge, we used a human metabolic model [28] that describes metabolic pathways in eight organs in mechanistic detail by enzyme kinetic equations. Variation of disease-relevant parameters generated different subject groups (i.e., control versus diseased). Through extensive computational experiments, we assess the performance of analysis of *fasting-state* data (using PCA), *T0-corrected* data (using

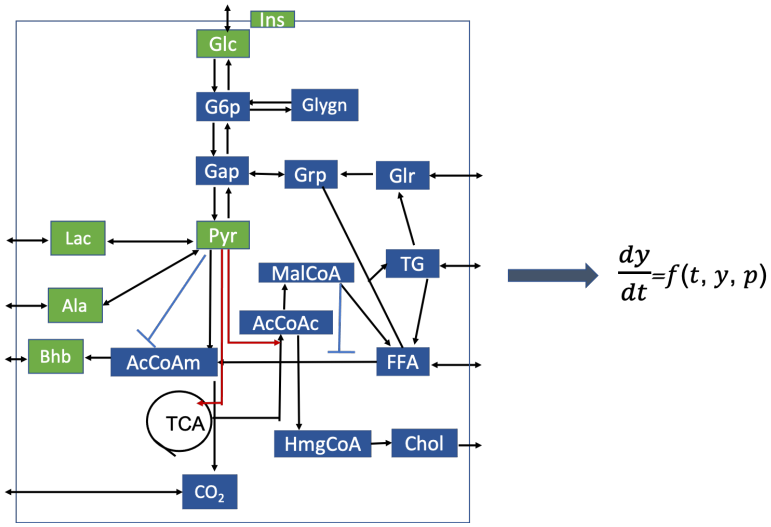

Fig 2. Metabolic network considered in each organ in the human whole-body model except for the pancreas; see [28] for more details.

a CP model) and *full-dynamic* data (using a CP model). We demonstrate that (i) CP models of postprandial metabolomics data reveal meaningful underlying patterns, (ii) for understanding metabolic differences among subject groups, it is crucial to analyze both *fasting-state* and *T0-corrected* data, (iii) depending on the nature of the subject group structure, the best performance in terms of revealing subject groups may be achieved by CP models of *T0-corrected* or *full-dynamic* data, and (iv) patterns extracted by CP models are reliable (i.e., consistently observed in a number of different settings such as when subsets of subjects are left-out, in the presence of a higher level of within-group variation, and with an unbalanced number of control and diseased subjects). Finally, we illustrate the proposed approach for real postprandial metabolomics data analysis from the COPSAC_{2000} (Copenhagen Prospective Studies on Asthma in Childhood) cohort [29] and discuss the patterns revealing metabolic differences among subjects in terms of their response to a meal challenge test.

Materials and methods

Simulated postprandial metabolomics data

Human whole-body metabolic model

To generate simulated postprandial metabolomics data, we consider a human whole-body metabolic model proposed by Kurata [28]. The model is defined by a set of ordinary differential equations, with metabolites as variables and kinetic constants as parameters. Consisting of 202 metabolites, 217 reaction rates and 1,140 kinetic parameters, this multi-scale and multi-organ model is the largest, comprehensive, and highly predictive kinetic model of the whole-body metabolism [28]. It describes each reaction with a reversible Michaelis-Menten type rate equation and includes the action of insulin and glucagon, key hormones that govern the response to a meal (Fig 2). The meal in this simulated model from [28] includes 87 grams (g) carbohydrate and 33 g fat, and is given after an overnight fasting.

Generation of the simulated data

To test whether our proposed unsupervised approach is able to reveal different subject groups, we generate simulated data using two types of variation: (i) between-group variation and (ii) within-group variation. The between-group variation is introduced by changing a specific parameter, i.e., Km_Ins_B_M or Km_inssyn_Glc_B, in the differential equations, as demonstrated in [28]. These two parameters are used to regulate the insulin-stimulated glucose uptake in skeletal muscle or the glucose-stimulated insulin secretion by the pancreas, respectively. Each type of between-group variation mimics one disease, which is as follows [28]:

- *Insulin resistance in skeletal muscle*: It is used for the study of type 2 diabetes mellitus and simulated by multiplying the default Km_Ins_B_M with 1.5,
- *Beta-cell dysfunction*: Its extreme case is type 1 diabetes mellitus and it is simulated by multiplying the default Km_inssyn_Glc_B with 1.1.

For the within-group variation, we randomly perturb the kinetic constants in the liver (see Supplemental S1 File for a list of perturbed parameters). The perturbation level is denoted by α. For example, $\alpha = 0.2$ indicates that related kinetic constants are set to be random parameters ranging from $(100 - 20)\%$ to $(100 + 20)\%$ of their default values.

Based on these definitions of between and within-group variations, we generate data for each subject as follows:

1. Get the 10-hour *fasting* concentrations for each individual (one individual has one set of random kinetic constants) by running the human whole-body metabolic model with the default initial values of model variables in [28], with an exception of the initial concentrations for particular metabolites presented in the next paragraph;
2. Start the meal challenge, i.e., run the human whole-body model using each individual's 10-hour *fasting* state, and take the concentrations of metabolites at time points $t = [0, 0.25, 0.5, 1, 1.5, 2, 2.5, 4]$ hours (with $T_0 = 0$h, $T_1 = 0.25$h, $\cdots$, $T_7 = 4$h).

We choose the above time points to match the time samples in the real data, which we use to assess how realistic the simulations are (see Section *Comparison of the simulated data with real meal challenge data*). In step one, we set initial values of Insulin (Ins) and blood metabolites Glucose (Glc), Pyruvate (Pyr), Lactate (Lac), Alanine (Ala), β-hydroxybutyrate (Bhb), Triglyceride and total Cholesterol to the median of fasting concentrations in the real data. Although the metabolic model involves 202 metabolites (including hormones) in different organs, we only consider hormone Ins and blood metabolites Glc, Pyr, Lac, Ala and Bhb since they are also measured in the real data. In addition, they are involved in the same metabolic network (see Fig 2), which makes the comparison of real and simulated data easier. When simulating data for a diseased subject, we use the parameter values given for *insulin resistance* and *beta-cell dysfunction*; otherwise, default values for parameters Km_Ins_B_M and Km_inssyn_Glc_B are used to simulate data for control subjects.

The simulated data from multiple subjects is arranged as a three-way array in the form of # subjects $\times$ 6 metabolites$\times$ # time points, as in Fig 1.

Comparison of the simulated data with real meal challenge data

We compared the simulated data using a real data set, which corresponds to Nuclear Magnetic Resonance (NMR) spectroscopy measurements of plasma samples collected

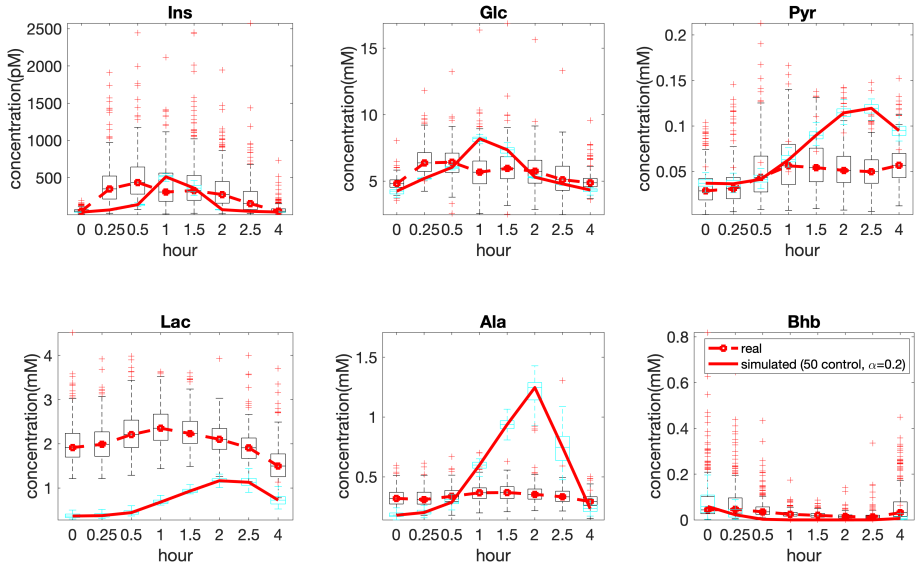

Fig 3. Median concentrations across all subjects following a meal challenge test. The standard meal in the real data includes 60 g palm olein, 75 g glucose and 20 g protein [30] and is given after overnight fasting, while the meal in simulations contains 87 g glucose and 33 g fat after 10-hour fasting.

during a meal challenge test from the COPSAC_{2000} cohort. The real data is not publicly available but may be shared by COPSAC through a collaboration agreement. The study was conducted in accordance with the Declaration of Helsinki and was approved by The Copenhagen Ethics Committee (KF 01-289/96 and H-16039498) and The Danish Data Protection Agency (2008-41-1754). Written consent was obtained from the participants. The cohort considered in this work consists of 299 healthy 18-year-old subjects (144 males and 155 females). The blood samples were collected at eight time points following an overnight fasting during the fasting and postprandial states, i.e., at $t = [0, 0.25, 0.5, 1, 1.5, 2, 2.5, 4]$h. Over two hundred features were measured. We select the six features mentioned in Section *Generation of the simulated data* since these are the ones available in both real and simulated data.

Time profiles of metabolites in simulated and real data match well for most metabolites except for Pyr and Lac, where we noticed deviations (See Supplemental S1 Fig. The simulated Pyr differed most from the standard reference range $[0.04, 0.1]$mmol/L. To get a better correspondence for the initial concentrations, we performed a sensitivity analysis and tuned the parameters related to Pyr and Lac (see Supplemental S2 Fig). After parameter tuning, all initial (fasting) concentrations, except Lac, corresponded well between the real and simulated data (see Fig 3). We note that also in [28] the measured concentration of Lac is higher than the simulated value (1 versus 0.5 mM). In our subjects, the Lac concentration is even higher, suggesting a difference between the cohorts. We did not necessarily expect a perfect correspondence between the real and simulated data throughout the time course since the simulated meal (taken from [28]) differed from the real meal (see Supplemental S1 Table); in addition, the large individual variability in the real data puts the discrepancy between the real and simulated data in perspective, as demonstrated in Fig 3. The simulated model is realistic for our study in the sense that we observe the responses of key metabolites upon the meal challenge, in the physiological range, which is what we are interested in.

CANDECOMP/PARAFAC (CP) model

The CP model, which stands for Canonical Decomposition (CANDECOMP) [20] and Parallel Factor Analysis (PARAFAC) [19], stems from the polyadic form of a tensor [31]. Similar to the matrix Singular Value Decomposition (SVD), the main idea of the CP model is to represent a tensor as the sum of a minimum number of rank-one tensors (Fig 1). The CP model has been successfully used in many disciplines, including data mining [17, 32], neuroscience [33, 34], chemometrics [35], and recently also in longitudinal omics data analysis [22] in terms of revealing the underlying patterns from complex data sets.

For a third-order tensor $\mathscr{X} \in \mathbb{R}^{I \times J \times K}$, an R-component CP model represents the tensor as follows:

$$\mathscr{X} \approx \sum_{r=1}^{R} \mathbf{a}_r \circ \mathbf{b}_r \circ \mathbf{c}_r, \tag{1}$$

where $\circ$ denotes the vector outer product, $\mathbf{A} = [\mathbf{a}_1 \ ... \ \mathbf{a}_R] \in \mathbb{R}^{I \times R}$, $\mathbf{B} = [\mathbf{b}_1 \ ... \ \mathbf{b}_R] \in \mathbb{R}^{J \times R}$, and $\mathbf{C} = [\mathbf{c}_1 \ ... \ \mathbf{c}_R] \in \mathbb{R}^{K \times R}$ are the factor matrices corresponding to each mode. Columns of the factor matrices, e.g., $\mathbf{a}_r, \mathbf{b}_r$, and $\mathbf{c}_r$ corresponding to the *rth component*, reveal the underlying patterns in the data. When assessing how well the CP model fits the data, we use the *explained variance* (also referred to as *model fit*) :

$$\text{Fit } (\%) = (1 - \frac{\left\| \mathscr{X} - \hat{\mathscr{X}} \right\|^2}{\| \mathscr{X} \|^2}) \times 100,$$

where $\hat{\mathscr{X}} := \sum_{r=1}^{R} \mathbf{a}_r \circ \mathbf{b}_r \circ \mathbf{c}_r$ is the data approximation based on the CP model, and $\| . \|$ denotes the Frobenius norm. A fit value close to 100% indicates that data $\mathscr{X}$ is explained well by the model; otherwise, there is an unexplained part left in the residuals.

The CP model has been widely used in applications as a result of its uniqueness property, i.e., factors are unique up to permutation and scaling ambiguities under mild conditions, without imposing additional constraints such as orthogonality [16, 21]. This uniqueness property facilitates interpretation. In the CP model, each rank-one component $(\mathbf{a}_r, \mathbf{b}_r, \mathbf{c}_r)$, i.e., rth column of factor matrices in all modes, can be interpreted, for instance, in terms of identifying groups of subjects (subjects with similar coefficients in $\mathbf{a}_r$) positively or negatively related to specific sets of metabolites (metabolites with large coefficients in $\mathbf{b}_r$) following certain temporal profiles (given by $\mathbf{c}_r$). We normalize vectors $(\mathbf{a}_r, \mathbf{b}_r, \mathbf{c}_r)$ to unit norm when we interpret the factors. Due to the scaling ambiguity in the CP model, the norms can be absorbed arbitrarily by the vectors as long as the product of the norms of the vectors stays the same. In the presence of missing entries, which is common in applications, it is still possible to analyze such incomplete data using a CP model [36, 37].

The selection of the number of components (i.e., R) when fitting a CP model is a challenging task [16, 38], and an active research topic [39]. Among existing approaches, we make use of the model fit and the core consistency diagnostic [40]. In addition, we choose the number of components based on the interpretability of the model and replicability of the factors [39, 41] in subsets of the data (see supplemental S2 File for details about the selection of number of components.)

Analysis approach

We analyze each postprandial metabolomics data set using three methods: (i) PCA of the *fasting-state* data, (ii) CP model of the *T0-corrected* data, and (iii) CP model of the *full-dynamic* data. We compare the *fasting-state* analysis with *T0-corrected* analysis to

	Individual Variation	
insulin resistance	$\alpha = 0.2$	balanced
		unbalanced
	$\alpha = 0.4$	balanced
		unbalanced
beta-cell dysfunction	$\alpha = 0.2$	balanced
		unbalanced
	$\alpha = 0.4$	balanced
		unbalanced

Table 1. Eight simulated data sets generated using different settings.

understand metabolic differences between these two states. We compare these three approaches to obtain a better picture in terms of subject group differences and underlying metabolic mechanisms.

Experimental set-up and implementation details

In our experiments with simulated data, we consider the analysis of eight data sets generated using different types of between-group variation, different levels of individual variations, and balanced or unbalanced groups (see Table 1 for a complete list of data sets). In the balanced case, there are 50 controls and 50 diseased subjects; in the unbalanced case, there are 70 control and 30 diseased subjects.

Before the CP analyses, the three-way data is preprocessed by centering across the *subjects* mode (to remove the common intercept from all subjects) and then scaling within the *metabolites* mode (to adjust for scale differences in different metabolites), i.e., dividing by the root mean squared value of each slice in the *metabolites* mode (see [42] for details about preprocessing multiway arrays). Before PCA, the *fasting-state* data is preprocessed similarly, i.e., centered and scaled.

For fitting CP models, we use `cp-opt` [43] and `cp-wopt` [37] from the Tensor Toolbox version 3.1 [44] with the Limited Memory BFGS optimization algorithm. `cp-wopt` uses weighted optimization [37] for fitting CP to incomplete data. For PCA, we use the `svd` function from MATLAB (if the data is incomplete, weighted optimization as in cp-wopt is used). Multiple random initializations are used to avoid local minima when fitting CP models and with weighted optimization. All experiments are performed in MATLAB 2020a. Simulated data sets in Table 1 and example scripts are available in the GitHub repository for the paper: `https://github.com/Lu-source/project-of-challenge-test-data`.

Results

CP models extract similar factors from the simulated vs. real meal challenge data

Since subjects in the real data are considered healthy, we expect that the CP model extracts similar patterns in *metabolites* and *time* modes from real data (299 subjects) vs. the simulated data with only the 50 control subjects ($\alpha = 0.2$). Patterns extracted from the *subjects* mode are omitted since the *subjects* mode corresponds to different individuals in simulated vs. real data. Fig 4 shows that the 3-component CP model of

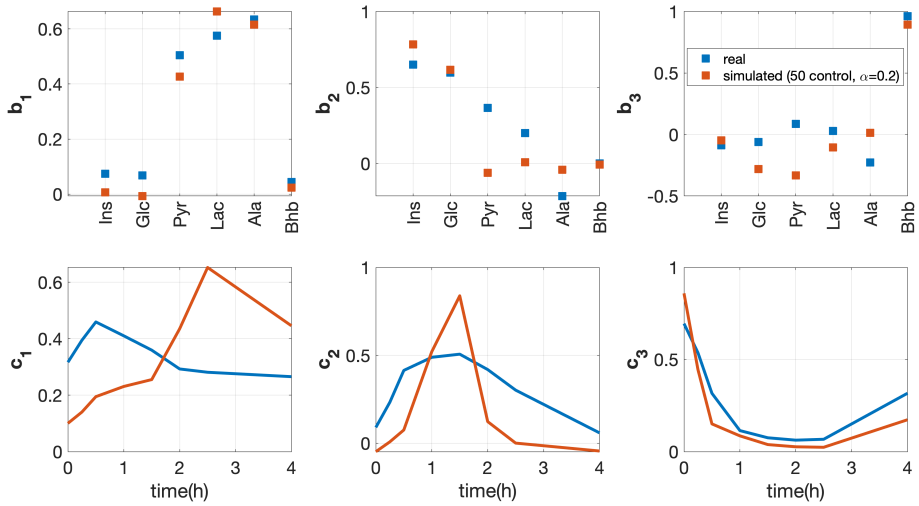

Fig 4. Factors in the *metabolites* (top plots) and *time* (bottom plots) modes extracted from the real vs. simulated data using a 3-component CP model. Model fits for the real and simulated data are 50.3% and 71.6%, respectively.

each data set reveals similar patterns from the *metabolites* and *time* modes, to some extent.

The first component ($\mathbf{b}_1$ and $\mathbf{c}_1$) in Fig 4 mainly models metabolites Pyr, Lac and Ala (i.e., metabolites with large coefficients) which share similar dynamic patterns, i.e., being accumulated and then consumed. It makes sense that these three metabolites stay close since they are tied to each other with reactions Pyr↔Lac and Pyr↔Ala as shown in the pathway in Fig 2. However, we observe different peak heights and different time points for the highest peak in the *time* mode in real vs. simulated data. The different peak heights are possibly because meal compositions are different in real vs. simulated data. The different time points at the highest peak may be due to the fact that different individuals reach the highest peak at different time in the real data, and the first component of real data (with $\mathbf{c}_1$) captures the temporal profiles of a group of subjects with the highest peak appearing at around 0.5h in metabolites Lac, Ala and Pyr (see supplemental S3 File for details).

The second component (see $\mathbf{b}_2$ and $\mathbf{c}_2$ in Fig 4) mainly captures Ins and Glc, which are accumulated and then consumed, after the meal challenge but at a different speed than Lac and Ala. However, we observe that the coefficient for Pyr is significantly different in real vs. simulated data. For the simulated data, the coefficient of Pyr is almost zero since the time point at the highest peak for all individuals in the simulated data is the same for each metabolite, and Pyr reaches to the highest peak at different time point compared with Ins and Glc. On the other hand, in real data, there are several subjects with dynamic patterns of Pyr reaching the highest peak at the same time point compared with Ins and Glc (see supplemental S3 File for more details). This results in a positive coefficient for Pyr in $\mathbf{b}_2$ in real data.

The third component ($\mathbf{b}_3$ and $\mathbf{c}_3$ in Fig 4) mainly models Bhb, which behaves differently from other metabolites after a meal challenge, i.e., being consumed first and then getting accumulated. This behaviour has been observed in a consistent way in both real and simulated data.

Insulin-resistant vs. control group with low within-group variation: *fasting* vs. *T0-corrected* analysis reveals metabolic differences and *T0-corrected* analysis performs better than *full-dynamic* analysis in terms of revealing group differences

Fasting-state analysis

PCA of the *fasting-state* data captures the subject group separation. The scatter plot of PC3 (the unpaired t-test using PC3 gives a p-value of 2×10^{-9}) and PC5 (p-value of 2×10^{-7}) in Fig 5 shows the best group separation. Note that PC3 and PC5 together explain only 21% of the data, indicating that the individual variation may dominate the total variation in the data. Fig 5 demonstrates that all metabolites except Ins and Glc are related to the subject group separation at the *fasting* state. Among them, Pyr contributes the most and is negatively related to the diseased group (i.e., the diseased group has mainly positive (negative) score values, and Pyr has a negative (positive) coefficient on PC3 (PC5)). This negative association indicates that the diseased group has lower concentration of Pyr at the *fasting* state. This results from a lower insulin-stimulated glucose uptake into the skeletal muscle in the *insulin-resistant* group, leading to less conversion of glucose into pyruvate.

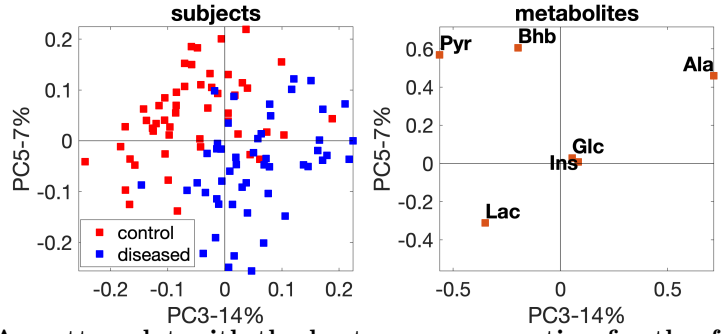

Fig 5. PCA scatter plot with the best group separation for the *fasting-state* data with *insulin-resistant* and control groups, and $\alpha = 0.2$.

T0-corrected analysis

We choose the 4-component CP model for the *T0-corrected* data (see supplemental S2 File for the selection of number of components). This model captures the subject group separation, as shown in Fig 6 (*subjects* mode). Among all components, the fourth component gives the best subject group separation (see the comparison of $\mathbf{a}_4$ with $\mathbf{a}_1$, $\mathbf{a}_2$ and $\mathbf{a}_3$). In the *metabolites* mode (see $\mathbf{b}_4$), metabolite Pyr has the largest coefficient, followed by Glc, while others have almost zero coefficients. In the *time* mode, $\mathbf{c}_4$ captures the dynamic behavior of mainly Pyr, i.e., it increases first and then slightly decreases. The increase of Pyr may be due to the glycolysis after the meal intake and its decrease afterwards may result from its conversion to other metabolites, e.g., Bhb, Lac and Ala, as shown in the pathway plot (Fig 2). $\mathbf{a}_4$, $\mathbf{b}_4$ and $\mathbf{c}_4$ together indicate that the concentration of Pyr increases more in the *insulin-resistant* group than in the control group; this suggests that the *T0-corrected* Pyr is positively related to the diseased group. Compared with $\mathbf{a}_4$, $\mathbf{a}_1$ and $\mathbf{a}_2$ reveal a weaker subject group separation due to the dynamic behavior of Lac & Ala (see $\mathbf{b}_1$ and $\mathbf{c}_1$) and Ins & Glc (see $\mathbf{b}_2$ and $\mathbf{c}_2$), respectively. Without capturing any group separation (see $\mathbf{a}_3$), the third component reveals that metabolite Bhb (it has the largest coefficient on $\mathbf{b}_3$ while others have almost zero coefficients) responds differently from the other metabolites after the meal intake (see $\mathbf{c}_3$ vs. $\mathbf{c}_1$, $\mathbf{c}_2$ and $\mathbf{c}_4$), i.e., it decreases first and then slowly increases,

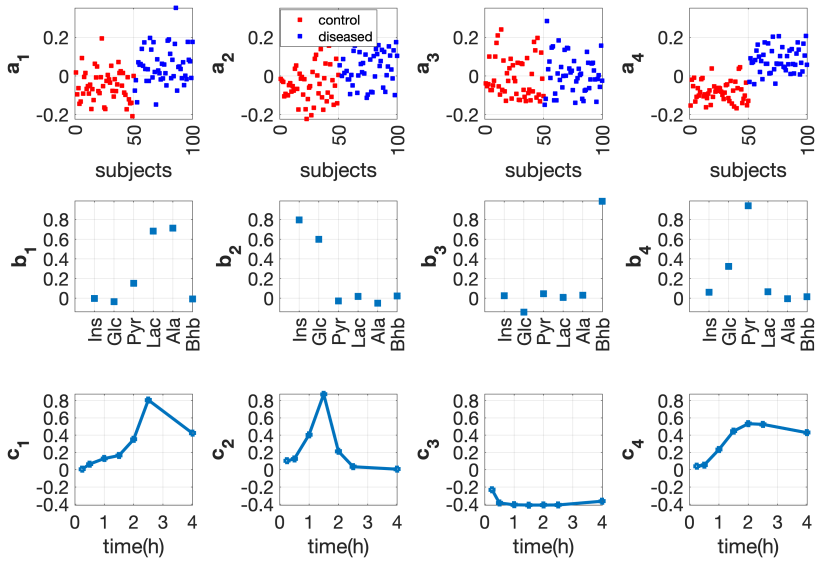

Fig 6. Factors of the 4-component CP model extracted from the *T0-corrected* data with *insulin-resistant* and control groups, and $\alpha = 0.2$.

as also shown in an earlier study [45].

Full-dynamic analysis

Fig 7 demonstrates the 4-component CP model of the *full-dynamic* data. This model captures both the *fasting-state* information ($\mathbf{c}_4$ reveals a constant temporal profile) and the *T0-corrected* information (i.e., the first and second components). The first component, i.e., $\mathbf{a}_1$, $\mathbf{b}_1$ and $\mathbf{c}_1$ together, and the second component, i.e., $\mathbf{a}_2$, $\mathbf{b}_2$ and $\mathbf{c}_2$ together, reveal the positive relation of Lac, Ala & Pyr and Ins & Glc with the diseased group and their dynamic response after the meal intake, respectively. The fourth component shows that Pyr negatively relates with the diseased group, i.e., the diseased group has negative coefficients in the *subjects* mode while Pyr has a positive coefficient in the *metabolites* mode.

Comparison of three analysis approaches

Through three analysis approaches, we observe four underlying mechanisms related to (i) Pyr, (ii) Ins & Glc, (iii) Lac, Ala & Pyr, and (iv) Bhb.

Pyr is identified by all methods as an essential metabolite related to the subject group separation. However, *fasting-state* vs. *T0-corrected* analysis reveals a different relation between Pyr and the diseased group. This, in turn, results in *T0-corrected* analysis performing better than *full-dynamic* analysis in terms of revealing group differences (see the comparison of the *subjects* mode in Fig 6 and 7). The best separation in *T0-corrected* analysis is given by the fourth component, where Pyr has the dominant coefficient in the *metabolites* mode. The left panel of Fig 8 shows that although the diseased group has a lower concentration of Pyr at the *fasting state*, Pyr accumulates much faster in the diseased group during the postprandial state (especially from 0.5h to 2h). In this sense, subtracting the *fasting-state* data from each time slice of the *full-dynamic* data leads to a more evident group difference between control vs. diseased subjects, as demonstrated in the right panel of Fig 8.

The other mechanisms, (ii) Ins & Glc, (iii) Lac, Ala & Pyr, and (iv) Bhb, are captured through similar patterns in both *T0-corrected* and *full-dynamic* analysis.

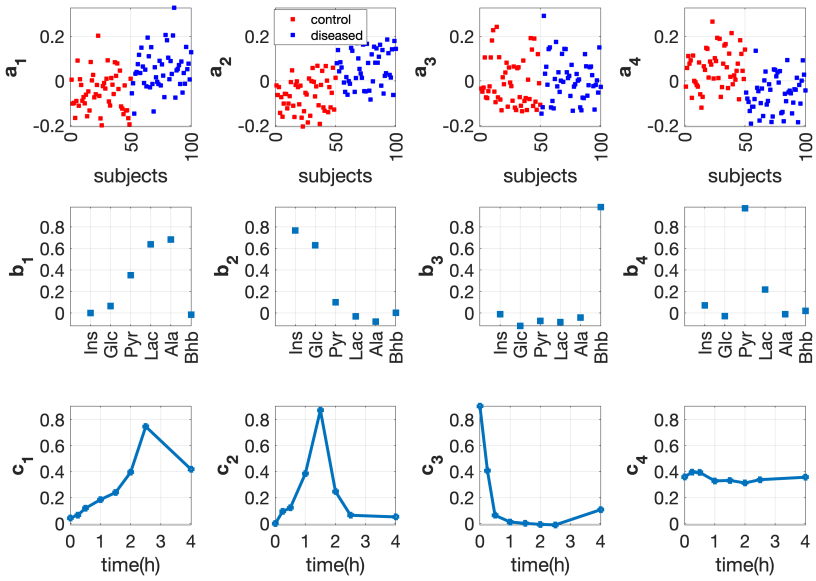

Fig 7. Factors of the 4-component CP model extracted from the *full-dynamic* data with *insulin-resistant* and control groups, and $\alpha = 0.2$.

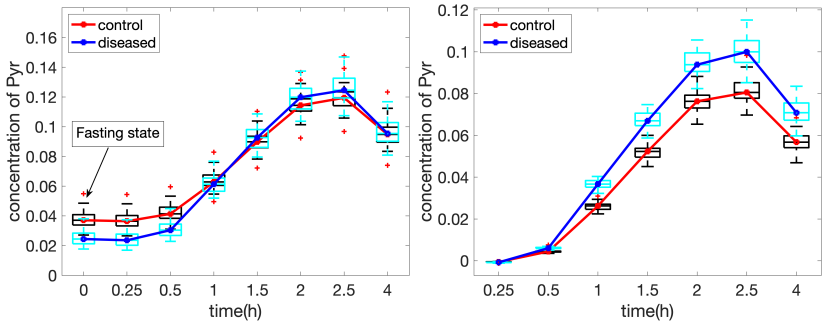

Fig 8. Median time profiles of Pyr for the raw *full-dynamic* data (Left panel) and *T0-corrected* data (Right panel) with *insulin-resistant* vs. control group and $\alpha = 0.2$.

Beta-cell dysfunction vs. control group with low within-group variation: *fasting* vs. *T0-corrected* analysis reveals metabolic differences and *full-dynamic* analysis performs better than *T0-corrected* analysis in terms of separating subject groups

Fasting-state analysis

The *fasting-state* analysis captures the subject group separation. The scatter plot of PC3 (with p-value of 8×10^{-7} from the unpaired t-test) and PC5 (with p-value of 2×10^{-8}) gives the best separation between the groups (Fig 9). Fig 9 also shows that metabolites Glc and Pyr contribute the most since they have large absolute coefficients along the discrimination direction (line $y = x$). In addition, it is shown that metabolite Glc (Pyr) is positively (negatively) related to the diseased group. This is consistent with Supplemental S3 Fig, which shows that the diseased group has a higher concentration of Glc and a lower concentration of Pyr at the *fasting state* compared with the control group. The higher plasma Glc in the diseased group results from inadequate glucose sensing to stimulate insulin secretion (*beta-cell dysfunction*). Due to

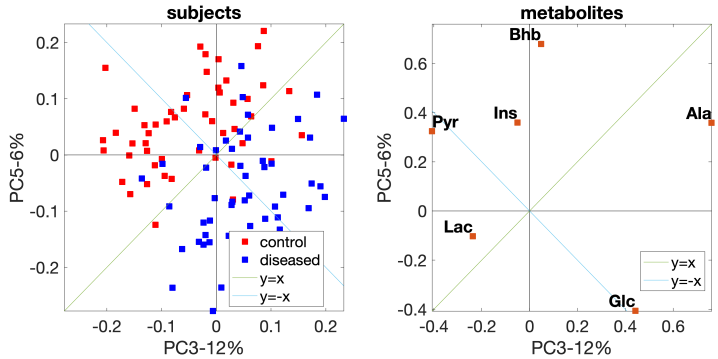

Fig 9. PCA scatter plot with the best group separation for the data set with *beta-cell dysfunction* and control groups, and $\alpha = 0.2$.

this inefficient secretion, glycolysis becomes less efficient, and less Pyr is produced, leading to a lower level of plasma Pyr in the diseased group.

T0-corrected analysis

We choose the 4-component CP model for the *T0-corrected* data. This model captures the subject group separation, and the best separation is achieved by $\mathbf{a}_2$ (see Fig 10). In the *metabolites* mode ($\mathbf{b}_2$), Ins has the largest coefficient followed by Glc, while other metabolites almost have no contribution. This indicates that the dynamic changes of Ins and Glc contribute to the subject group separation, and Ins is the most significant one. Ins is shown to be negatively associated with the *beta-cell dysfunction* group. It makes sense that Glc stays close to Ins and shares a similar dynamic pattern as Ins (see Supplemental S4 Fig) since Ins and Glc regulate each other. In the *time* mode, $\mathbf{c}_2$ captures the dynamic pattern shared by Ins and Glc, i.e., an increase after the meal intake and then a decrease due to the glycolysis. $\mathbf{a}_1$ (with p-value of 8×10^{-5}) and $\mathbf{a}_4$ (with p-value of 2×10^{-4}) capture weak group separation in the *subjects* mode. In the *metabolites* mode, $\mathbf{b}_1$ captures the fact that Pyr, Lac and Ala respond to the meal challenge similarly, and this makes sense since they are close to each other, as shown in the pathway in Fig 2.

Full-dynamic analysis

We choose the 4-component CP model to analyze the *full-dynamic* data, with factor plots shown in Fig 11. $\mathbf{a}_4$ reveals the subject group differences best. In the *metabolites* mode ($\mathbf{b}_4$), metabolites Glc and Pyr have the largest coefficients in terms of absolute values. This component also reveals the positive (negative) relation of metabolite Glc (Pyr) with the diseased group (i.e., the diseased group has negative coefficients in the *subjects* mode while metabolite Glc (Pyr) has a positive (negative) coefficient in the *metabolites* mode). In the *time* mode, we observe a non-constant dynamic profile ($\mathbf{c}_4$) with a large coefficient at $t = 0$ comparable to the coefficients of other time points. This indicates that the fourth component captures a mixture of information from the *fasting* and *T0-corrected* states, and the *fasting-state* signal is relatively strong. The model also captures the pattern (the second component) in *T0-corrected* analysis (see $\mathbf{a}_2$, $\mathbf{b}_2$ and $\mathbf{c}_2$ in Fig 11), which shows that the beta-cell dysfunction group is negatively related with Ins.

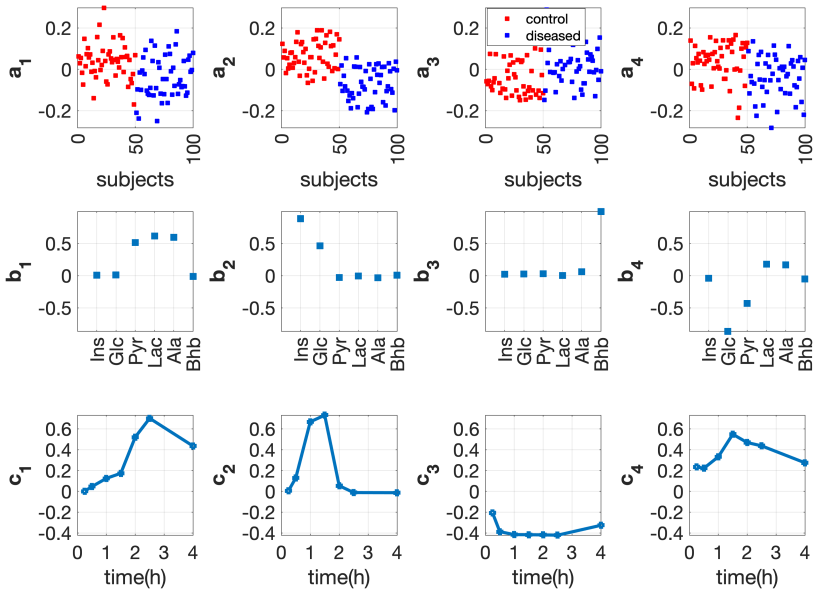

Fig 10. Factors of the 4-component CP model of *T0-corrected* data with *beta-cell dysfunction* and control groups, and $\alpha = 0.2$.

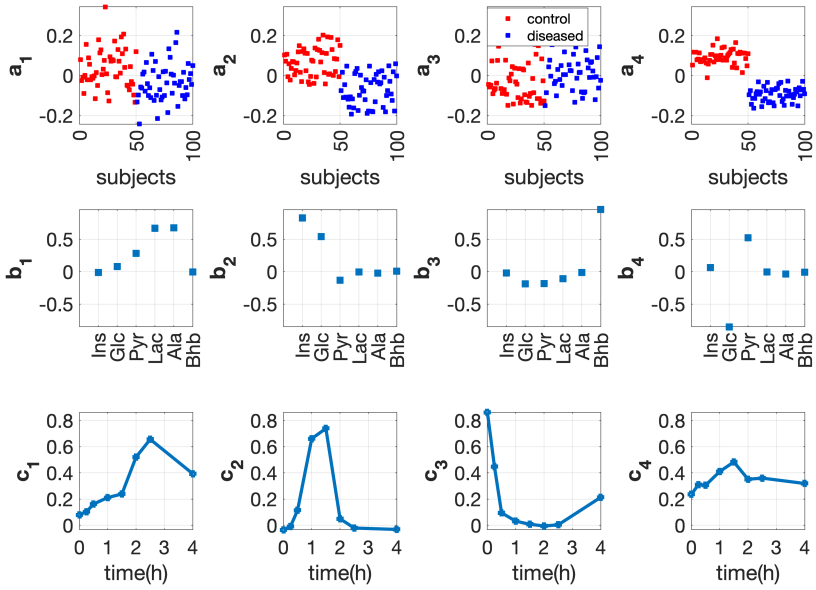

Fig 11. Factors of the 4-component CP model for *full-dynamic* data with *beta-cell dysfunction* and control groups, and $\alpha = 0.2$.

Comparison of three analysis approaches

In this case, we observe four underlying mechanisms related to (i) Glc & Pyr, (ii) Ins & Glc, (iii) Lac, Ala & Pyr, and (iv) Bhb.

While both *fasting-state* analysis and *T0-corrected* analysis can separate subject groups, the mechanisms responsible for group separation are different, with Glc & Pyr playing a role at the *fasting-state* analysis while Ins & Glc playing the main role in the *T0-corrected* analysis. We also observe that *full-dynamic* analysis outperforms the other two approaches in terms of capturing the subject groups (see the comparison of Fig 10 and 11). The best separation in the *full-dynamic* analysis is provided by the fourth

component, which captures a mixture of the information from the *fasting* and *T0-corrected* states. The good separation is because the Glc & Pyr signal at the *fasting* state gets stronger through the dynamic information. This is consistent with the more evident group difference observed at the postprandial state from the time profiles of Glc (see Supplemental S3 Fig).

The other mechanisms (iii) Lac, Ala & Pyr, and (iv) Bhb are captured similarly using both *T0-corrected* and *full-dynamic* data analysis.

The proposed analysis approach reveals metabolic aberrations

The crucial question in an unsupervised analysis is whether such an analysis can find groupings among the subjects pointing to metabolic differences or even metabolic deficiencies. The two studied metabolic deficiencies clearly show different patterns for the metabolites Ins, Glc and Pyr in the different analyses. These different patterns can be understood using the underlying metabolic network, thereby validating the power of the data analysis approach in its ability to discriminate between different types of metabolic differences. Although we showed this only for two metabolic deficiencies, we expect this property to hold also for other types of metabolic differences, especially when -in real-data cases- more than six metabolites are being considered.

CP models reveal stable patterns

Within-group variation can be enormous in real data making data analysis more challenging. For example, large within-group variations in healthy subjects might cover the changes of metabolites in response to diseases when exploring biomarker candidates [46]. Our numerical experiments demonstrate that CP models reveal stable patterns even when the level of individual variation is increased. Fig 12 shows the CP factors extracted through *T0-corrected* analysis from two data sets generated with *insulin-resistant* and control groups using two different levels of individual variation, i.e., $\alpha = 0.2$ and $\alpha = 0.4$.

We quantify the similarity of CP factors in the *metabolites* and *time* modes using the factor match score (FMS) defined as follows:

$$\mathrm{FMS} = \frac{1}{R}\sum_{r=1}^{R} \frac{|\mathbf{b}_r{}^{\mathsf{T}}\hat{\mathbf{b}}_r|}{\|\,\mathbf{b}_r\,\|\,\|\,\hat{\mathbf{b}}_r\,\|}\,\frac{|\mathbf{c}_r{}^{\mathsf{T}}\hat{\mathbf{c}}_r|}{\|\,\mathbf{c}_r\,\|\,\|\,\hat{\mathbf{c}}_r\,\|}$$

where $\mathbf{b}_r$, $\mathbf{c}_r$ and $\hat{\mathbf{b}}_r$, $\hat{\mathbf{c}}_r$ denote the rth column of factor matrices in *metabolites* and *time* modes extracted by CP models from two different data sets (after finding the best permutation of the columns). FMS values are between 0 and 1, and an FMS value close to 1 indicates high similarity between CP factors extracted from two different data sets.

In addition to different levels of individual variation, we consider data sets with an unbalanced number of control and diseased subjects. Supplemental S2 Table and S3 Table show that CP factors are similar for data sets using balanced vs. unbalanced samples, and using different levels of individual variations, with the smallest FMS value of 0.90.

Real data: the *fasting* and *T0-corrected* metabolism behave differently in terms of grouping subjects

We use the real data corresponding to NMR measurements of plasma samples collected during the meal challenge test from the COPSAC_{2000} cohort to demonstrate the application of the proposed analysis approach in real data analysis. For our analysis, we

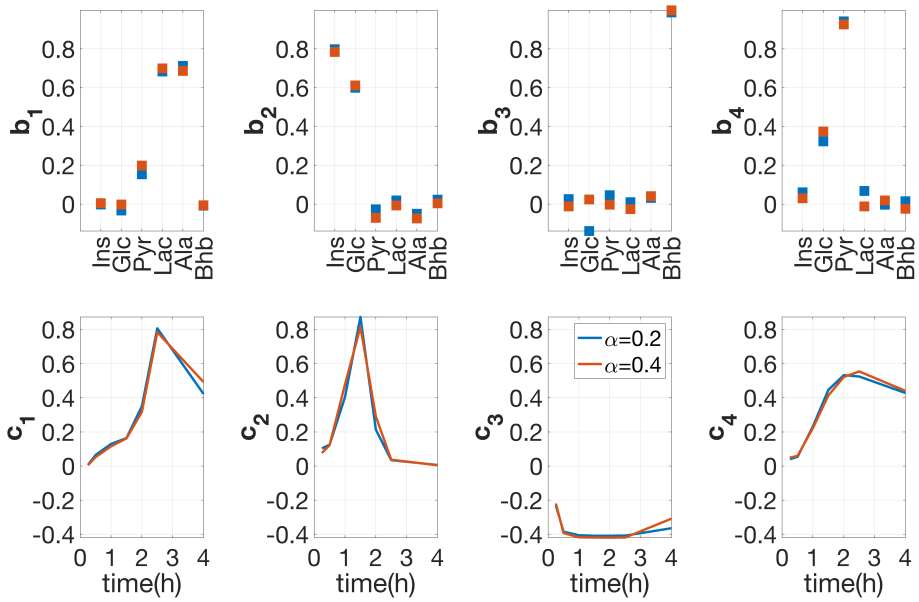

Fig 12. Comparison of the factors in the *metabolites* and *time* modes extracted from the *T0-corrected* data of two data sets with different levels of individual variation, $\alpha = 0.2$ vs. $\alpha = 0.4$, and 50 *insulin-resistant* subjects and 50 control subjects.

only consider males to eliminate potential interference due to gender difference (e.g., as reported in [5]) and include 162 features corresponding to metabolite concentrations as well as insulin and c-peptide measurements. We removed four outlier subjects (i.e., three subjects had extremely high levels of acetate, and one subject was marked by the model as an outlier due to a high leverage score and residual). The final data set to be analyzed is in the form of a third-order tensor: 140 subjects×162 metabolites× 8 time points. We preprocess the data in the same way as the simulated data, i.e., centering across the *subjects* modes and then scaling within the *metabolites* mode.

We carry out *fasting-state* analysis using PCA, and analysis of *T0-corrected* and *full-dynamic* data using a CP model to capture the underlying patterns in the data and reveal potential differences and similarities among subjects in terms of their response to the meal challenge. We include here the *fasting-state* and *T0-corrected* analysis since they together provide a better picture of the underlying patterns of *fasting* and *pure-dynamic* states. The analysis of *full-dynamic* data reveals a *fasting-state* component and a component similar to the component observed in the analysis of *T0-corrected* data; however, unlike in Fig 11, the *fasting-state* component in the *full-dynamic* analysis does not get support in the dynamic part; therefore, the *full-dynamic* analysis does not perform better. Here, we include a brief summary of our results, and a more comprehensive analysis (e.g., males vs. females) is the topic of ongoing research.

Fasting-state **analysis**

Fig 13 shows the scatter plots of PC1 and PC2 in the *subjects* and *metabolites* mode. In the *subjects* mode, PC1 captures a weak but statistically significant group difference with a p-value of 1×10^{-3} in terms of *lower* vs. *higher* BMI groups. In our data set, there are 10 underweight (BMI less than 18.5), 100 normal (BMI greater than or equal to 18.5 and less than 25.0), 21 overweight (BMI greater than or equal to 25.0 and less

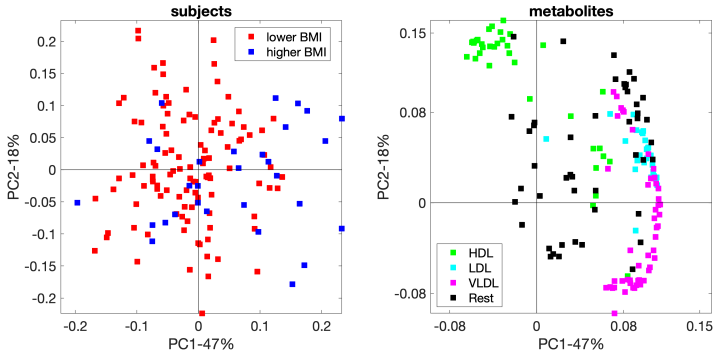

Fig 13. Real data. The scatter plot of PC1 and PC2 from the PCA model of the *fasting-state* data with 140 male subjects and 162 metabolites.

than 30.0) and 9 obese (BMI greater than or equal to 30.0) subjects. Due to too few subjects in some groups, we assign subjects with BMI less than 25.0 to the *lower* BMI group while the *higher* BMI group consists of subjects with BMI greater than or equal to 25.0. The right panel of Fig 13 shows the metabolites colored according to lipoprotein classes: high-density lipoproteins (HDL), low-density lipoproteins (LDL), and very low-density lipoproteins (VLDL), as well as the rest group containing the remaining metabolites. HDL, LDL, VLDL classes contain cholesterol (C), triglycerides (TG), phospholipids (PL), cholesteryl esters (CE), free cholesterol (FC), total lipids (L), particle concentrations (P) as S (small), M (medium), L (large), XL (very large) subclasses (also XS and XXL for VLDL). We observe that metabolites with large coefficients in the first component, i.e., mainly VLDLs and LDLs (magenta and cyan squares with high coefficients), are positively related to *higher* BMI group while HDLs (green squares) are negatively related to *higher* BMI group. This observation, in particular, for VLDL-C, LDL-C and HDL-C, is consistent with previous studies [47, 48].

T0-corrected analysis

We use a 2-component CP model to analyze the *T0-corrected* data (see details about the model selection in Supplemental S2 File) as shown in Fig 14. The second component is potentially interesting since it captures the dynamic challenge test profile and reveals a group difference in terms of BMI (with a p-value of 6×10^{-4}, the group difference is also illustrated using boxplots in Supplemental S5 Fig). From the *metabolites* mode ($\mathbf{b}_2$) of Fig 14, we observe that a group of VLDLs (mainly (L/XL/XXL)-VLDLs, i.e., the magenta squares over the line $y = 0.08$), and a few of HDLs, i.e., the green squares over the line $y = 0.08$, have positive large coefficients and are positively related to *higher* BMI group. On the other hand, a small group of VLDLs (mainly (S/M)-VLDLs) and LDLs, i.e., magenta and cyan squares around the line $y = -0.08$) have negative coefficients, and are negatively related to *higher* BMI. In the *time* mode, we observe a dynamic pattern with the highest peak appearing at around 2.5 hours. While statistically significant changes in time in lipoprotein subclasses have been previously reported after a meal intake across different subject groups [3], that has been done univariately - not providing the subgroup structure in the *metabolites* mode or the temporal profile we capture in Fig 14. While we have not observed any grouping as a result of other subgroups such as cholesterol (C), triglycerides (TG), that is the focus of future research. The first component mainly captures an earlier response potentially modelling differences among individuals.

When we compare the *fasting-state* and *T0-corrected* data analysis, we observe that some metabolites behave differently at *fasting* vs. *pure-dynamic* states. The clearest

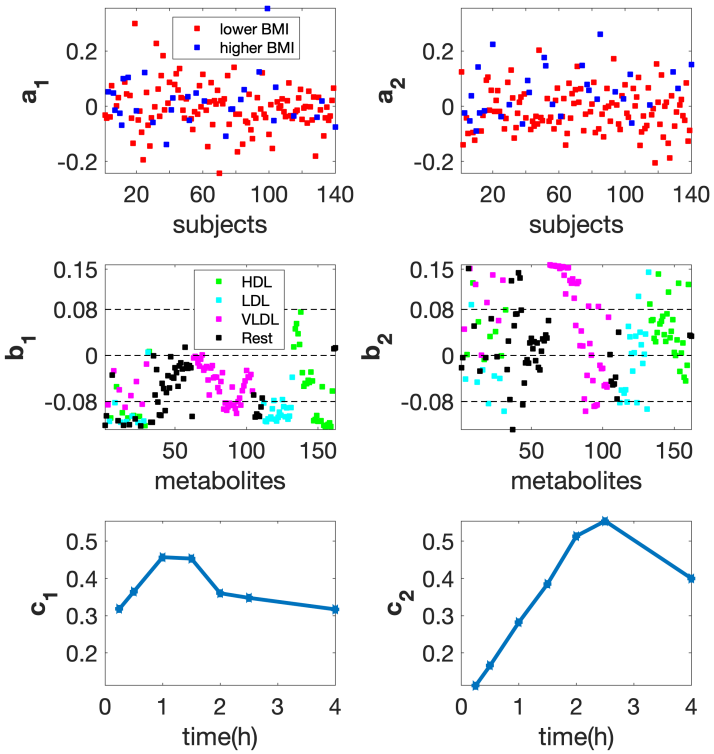

Fig 14. Real data. 2-component CP model of *T0-corrected* data with 140 subjects×162 metabolites× 7 time points. The model fit is 44.0%**.**

observation is that while almost all VLDLs show positive relation with *higher* BMI at the *fasting state*, in the *pure-dynamic* state, small vs. large VLDL subgroups behave differently. For instance, looking at the time profiles of S-VLDL-C, which has a high negative coefficient in Fig 14 in the second component, in the left panel of Supplemental S6 Fig, we see that the *higher* BMI group has a higher *fasting* S-VLDL-C, but the concentration of S-VLDL-C in the *higher* BMI group decreases much faster than the *lower* BMI group from 0.25h to 2.0h. This explains the different association of the *fasting-state* vs. *T0-corrected* S-VLDL-C with BMI groups.

Discussion

In this paper, we have proposed an unsupervised approach based on the CP model to improve the analysis of the postprandial metabolomics data. Using the simulated data with known ground truth, we have demonstrated the benefits of the proposed approach. One benefit is the extraction of the underlying patterns in all modes simultaneously, which presents the correlation within one mode and the association among all modes in one paradigm. In addition, we have shown that CP models could extract reliable patterns under various settings, e.g., even for data with considerable within-group variation. Another benefit is an overall picture of metabolic differences at the *fasting* vs. *T0-corrected* state, which can be obtained by using PCA for the *fasting-state* data and the CP model for the *T0-corrected* data analysis. Understanding such metabolic differences helps to explore the added value in the postprandial state due to metabolites' dynamic responses. This, in turn, provides insightful guidance in terms of analyzing baseline-corrected data or *full-dynamic* data in longitudinal analysis. The simulation studies indicate that such metabolic differences depend on the nature of the

between-group variation, which may be related to metabolic deficiency or aberration due to genetic variations in different groups of subjects. While our experiments rely on data sets consisting of a control group and a diseased group, the proposed analysis approach holds the promise to reveal subject group differences due to different diseases, e.g., *insulin-resistant* vs. *beta-cell dysfunction* vs. control group, as well as subgroups of diseases, e.g., *insulin-resistant* vs. less *insulin-resistant* vs. control group.

Although this paper focuses on the analysis of meal challenge test data, we expect the proposed approach to be suitable for other applications of time-resolved data analysis, for example, diet intervention data [49, 50] and other types of challenge test data such as exercise challenge tests [51]. A common feature of such data is that they are time-resolved and hold both the baseline and *pure-dynamic* information. The essential idea is to analyze the baseline data together with the baseline-corrected data to understand their differences. If group structures are detected, understanding such differences will facilitate better utilization of the time-resolved information.

A side product of our study is an approach to generate meaningful simulated postprandial metabolomics data. We use a comprehensive metabolic model to create such data. While the metabolic model was previously proposed, we tuned the model based on a comparison with our real data set including hundreds of subjects. Such simulated models may also be beneficial in terms of the optimal design of meal challenge tests.

Nevertheless, there are also several limitations in this study and possible future research directions. Using the model, we have only generated data where the concentration of each metabolite reaches the highest peak at the same time points for all subjects. However, in reality, time points at the highest peak vary from one subject to another. The main difficulty in generating such data is tuning the parameters while keeping the concentrations in reasonable ranges. Since the mathematical metabolic model involves 1140 parameters and 202 metabolites in eight different organs, parameter tuning is not trivial. Other limitations come from assumptions of the data analysis method. The CP model assumes that temporal patterns (i.e., $\mathbf{c}_r$) are the same across subjects as we have in the simulated data; however, in real data, we observe shifts in temporal profiles, e.g., highest peaks at different time points for different subjects. Furthermore, another assumption in the CP model is that the factor matrix in the *metabolites* modes is the same across all time slices. However, those factor matrices may change over time. To account for such subject-specific temporal profiles or time-evolving factors in the *metabolites* mode, alternative multiway methods such as the PARAFAC2 model [52] may prove useful as already shown for the analysis of neuroimaging signals [53–55] and in chemometrics [56].

Supporting information

S1 Fig. Median time profiles of the real vs. simulated (50 control subjects and $\alpha = 0.2$) data generated from the default human whole-body metabolic model.

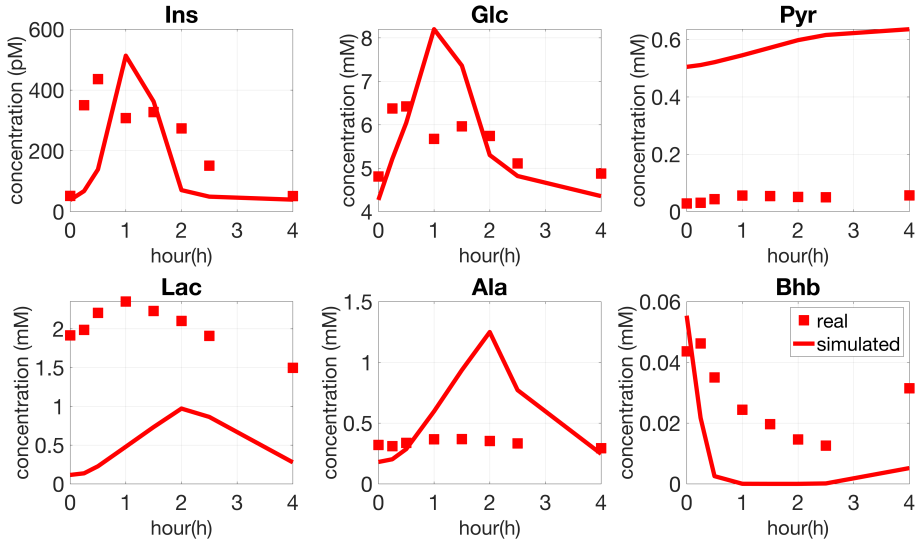

S2 Fig. Sensitivity analysis for metabolites Pyr (left panel) and Lac (right panel). We observed an apparent deviation of Pyr from the reference range $[0.04, 0.1]$ mmol/L using the default model shown in S1 Fig; therefore, we performed a sensitivity analysis (checking how the change of parameters related to Pyr will affect the change of its 10h-fasting concentration) to tune the parameters in the human whole-body model so that the 10h-fasting concentration of Pyr falls into the reference range. From the left panel in S2 Fig, we select to increase v-pyrt-pyr-B-A by 0.007 (the default value is 0) to obtain a significant decrease of the 10h-fasting Pyr. In addition, we increase Vdif-pyrt-pyr-B-L by 0.003 (the default value is 0) to make an adjustment. Although the right panel in S2 Fig indicates decreasing v-lact-lac-B-N or v-lact-lac-B-T will increase the 10h-fasting Lac, such an increase will lead to negative concentrations of Lactate in the brain (N) or other tissues (T). We make a minor adjustment to Lac by setting Vdif-lact-Lac-B-L to 12*0.08 (the default value is 12). Details about the equations and parameters related to Pyr and Lac can be found in [28].

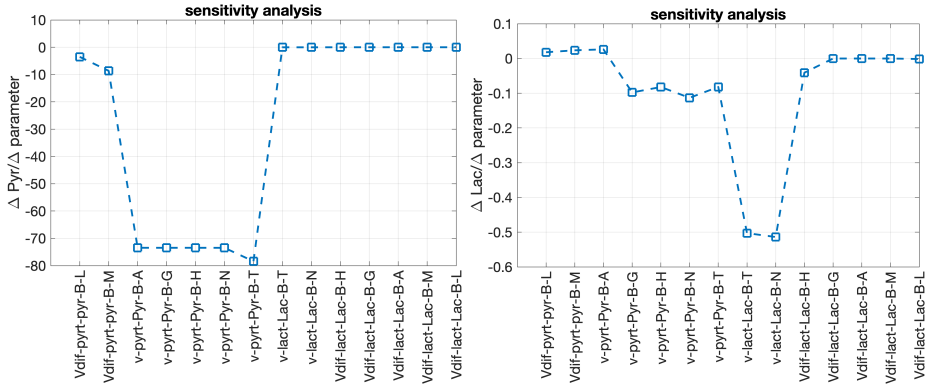

S3 Fig. Median time profiles of control vs. diseased group for the *full-dynamic* data generated with *beta-cell dysfunction* and $\alpha = 0.2$, where there are 50 control and 50 diseased subjects.

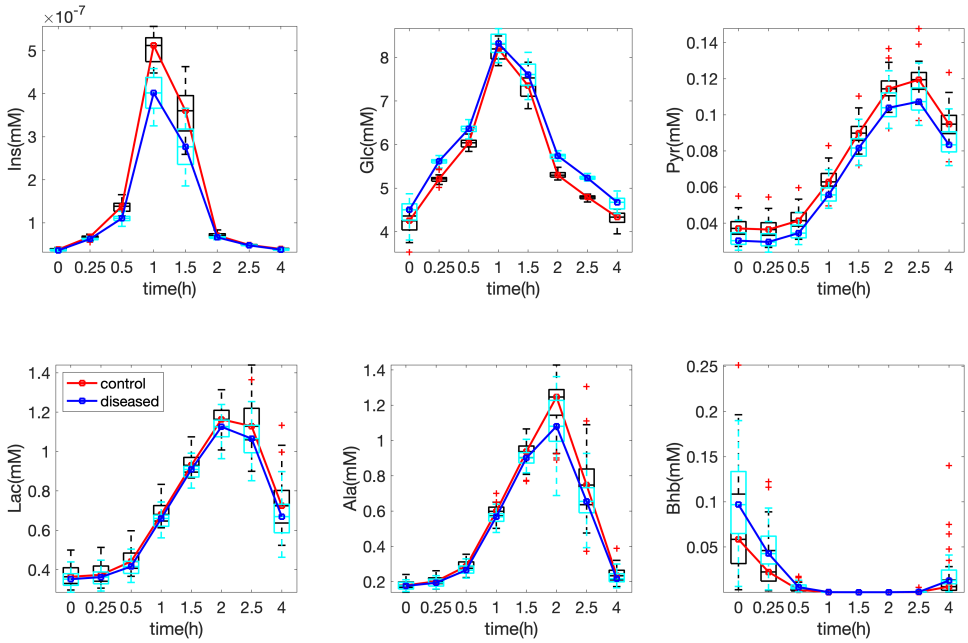

S4 Fig. Median time profiles of control vs. *beta-cell dysfunction* group for the *T0-corrected* data generated with $\alpha = 0.2$. The data contains 50 control and 50 diseased subjects.

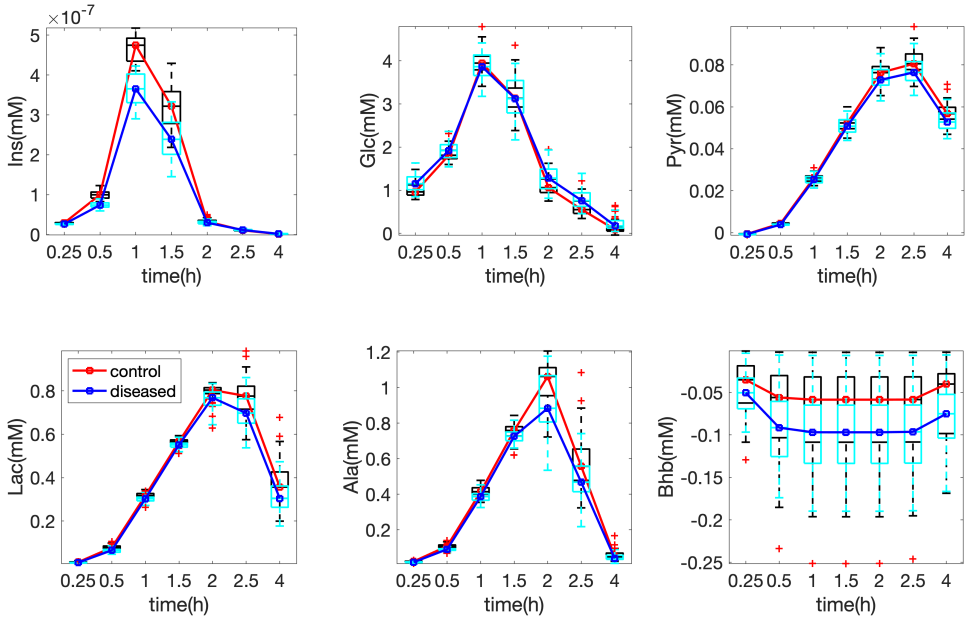

S5 Fig. Coefficients of subjects in *lower* vs. *higher* BMI group in the second component of the CP model of *T0-corrected* data. The group difference is statistically significant with a p-value of 6×10^{-4}.

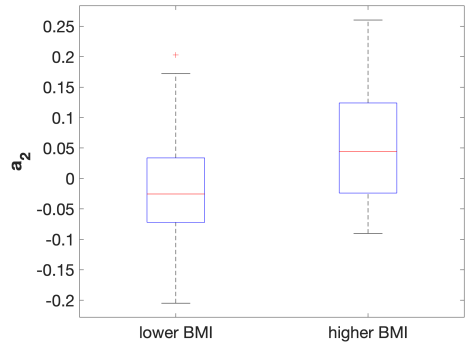

S6 Fig. Median time profiles of S-VLDL-C for the *higher* vs. *lower* BMI group. Left panel: raw *full-dynamic* data, and right panel: *T0-corrected* data. Red/blue lines correspond to the median time profiles across subjects in *lower*/*higher* BMI groups.

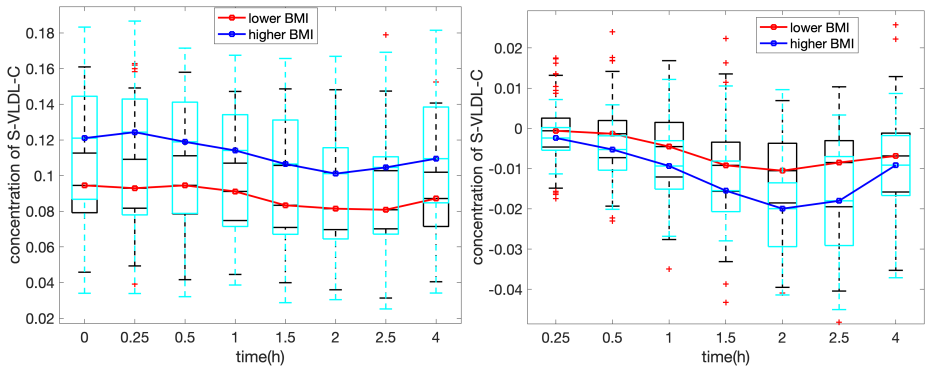

S1 File. A list of parameters perturbed for generating different individuals.

S2 File. Selection of the number of components in CP models.

S3 File. Details about the comparison of the CP factors for the simulated vs. real data.

S1 Table. Meal compositions of the real and simulated data.

	glucose (g)	fat (g)	protein (g)
real data	60	75	25
simulated data	87	33	0

S2 Table. *Full-dynamic data analysis*. Similarity between the CP factors (in *metabolites* and *time* modes) extracted from different data sets and the CP factors of the data set with $\alpha = 0.2$ and balanced samples.

	Individual Variation		R	FMS
insulin resistance	$\alpha = 0.2$	balanced	4	-
		unbalanced	4	1.00
	$\alpha = 0.4$	balanced	4	0.97
		unbalanced	4	0.97
beta-cell dysfunction	$\alpha = 0.2$	balanced	4	-
		unbalanced	4	1.00
	$\alpha = 0.4$	balanced	5	0.93
		unbalanced	5	0.90

S3 Table. *T0-corrected data analysis*. Similarity between the CP factors (in *metabolites* and *time* modes) extracted from different data sets and the CP factors of the data set with $\alpha = 0.2$ and balanced samples.

	Individual Variation		R	FMS
insulin resistance	$\alpha = 0.2$	balanced	4	-
		unbalanced	4	1.00
	$\alpha = 0.4$	balanced	4	0.99
		unbalanced	4	0.99
beta-cell dysfunction	$\alpha = 0.2$	balanced	4	-
		unbalanced	4	0.96
	$\alpha = 0.4$	balanced	5	0.91
		unbalanced	5	0.91

Acknowledgments

This research has been funded by Novo Nordisk Foundation Grant NNF19OC0057934 and Research Council of Norway project 300489.

References

1. Harte AL, Varma MC, Tripathi G, McGee KC, Al-Daghri NM, Al-Attas OS, et al. High fat intake leads to acute postprandial exposure to circulating endotoxin in type 2 diabetic subjects. Diabetes Care. 2012;35(2):375–382.

2. Wopereis S, Stroeve JHM, Stafleu A, Bakker GCM, Burggraaf J, van Erk MJ, et al. Multi-parameter comparison of a standardized mixed meal tolerance test in healthy and type 2 diabetic subjects: the PhenFlex challenge. Genes & Nutrition. 2017;12(21):1–14.

3. Wojczynski MK, Glasser SP, Oberman A, Kabagambe EK, Hopkins PN, Tsai MY, et al. High-fat meal effect on LDL, HDL, and VLDL particle size and number in the Genetics of Lipid-Lowering Drugs and Diet Network (GOLDN): an interventional study. Lipids in Health and Disease. 2011;10(181):1–11.

4. Lépine G, Tremblay-Franco M, Bouder S, Dimina L, Fouillet H, Mariotti F, et al. Investigating the Postprandial Metabolome after Challenge Tests to Assess

Metabolic Flexibility and Dysregulations Associated with Cardiometabolic Diseases. Nutrients. 2022;14(3):472.

5. Kumar AA, Satheesh G, Vijayakumar G, Chandran M, Prabhu PR, Simon L, et al. Postprandial Metabolism is Impaired in Overweight Normoglycemic Young Adults without Family History of Diabetes. Scientific Reports. 2020;10:353.

6. Zeevi D, Korem T, Zmora N, Israeli D, Rothschild D, Weinberger A, et al. Personalized nutrition by prediction of glycemic responses. Cell. 2015;163(5):1079–1094.

7. Berry SE, Valdes AM, Drew DA, Asnicar F, Mazidi M, Wolf J, et al. Human postprandial responses to food and potential for precision nutrition. Nature Medicine. 2020;26(6):964–973.

8. Müllner E, Röhnisch HE, Von Brömssen C, Moazzami AA. Metabolomics analysis reveals altered metabolites in lean compared with obese adolescents and additional metabolic shifts associated with hyperinsulinaemia and insulin resistance in obese adolescents: A cross-sectional study. Metabolomics. 2021;17(1):1–13.

9. Vis DJ, Westerhuis JA, Jacobs DM, van Duynhoven JP, Wopereis S, van Ommen B, et al. Analyzing metabolomics-based challenge tests. Metabolomics. 2015;11(1):50–63.

10. Smilde AK, Jansen JJ, Hoefsloot HC, Lamers RJA, Van Der Greef J, Timmerman ME. ANOVA-simultaneous component analysis (ASCA): a new tool for analyzing designed metabolomics data. Bioinformatics. 2005;21(13):3043–3048.

11. Harrington P, Vieira NE, Espinoza J, Nien JK, Romero R, Yergey AL. Analysis of variance–principal component analysis: A soft tool for proteomic discovery. Analytica Chimica Acta. 2005;544(1-2):118–127.

12. Thissen U, Wopereis S, van den Berg SA, Bobeldijk I, Kleemann R, Kooistra T, et al. Improving the analysis of designed studies by combining statistical modelling with study design information. BMC Bioinformatics. 2009;10(1):1–15.

13. Thiel M, Feraud B, Govaerts B. ASCA+ and APCA+: Extensions of ASCA and APCA in the analysis of unbalanced multifactorial designs. Journal of Chemometrics. 2017;31(6):e2895.

14. Martin M, Govaerts B. LiMM-PCA: Combining ASCA+ and linear mixed models to analyse high-dimensional designed data. Journal of Chemometrics. 2020;34(6):e3232.

15. Pellis L, van Erk MJ, van Ommen B, Bakker GCM, Hendriks HFJ, Cnubben NHP, et al. Plasma metabolomics and proteomics profiling after a postprandial challenge reveal subtle diet effects on human metabolic status. Metabolomics. 2012;8:347–359.

16. Kolda TG, Bader BW. Tensor decompositions and applications. SIAM Review. 2009;51(3):455–500.

17. Acar E, Yener B. Unsupervised Multiway Data Analysis: A Literature Survey. IEEE Transactions on Knowledge and Data Engineering. 2009;21(1):6–20.

18. Smilde A, Bro R, Geladi P. Multi-Way Analysis: Applications in the Chemical Sciences. West Sussex, England: Wiley; 2004.

19. Harshman RA. Foundations of the PARAFAC procedure: Models and conditions for an "explanatory" multimodal factor analysis. UCLA working papers in phonetics. 1970;16:1–84.

20. Carroll JD, Chang JJ. Analysis of individual differences in multidimensional scaling via an N-way generalization of "Eckart-Young" decomposition. Psychometrika. 1970;35(3):283–319.

21. Kruskal JB. Three-way arrays: rank and uniqueness of trilinear decompositions, with application to arithmetic complexity and statistics. Linear Algebra and its Applications. 1977;18(2):95–138.

22. Martino C, Shenhav L, Marotz CA, Armstrong G, McDonald D, Vázquez-Baeza Y, et al. Context-aware dimensionality reduction deconvolutes gut microbial community dynamics. Nature Biotechnology. 2021;39(2):165–168.

23. Gardlo A, Smilde AK, Hron K, Hrda M, Karlikova R, Friedecký D, et al. Normalization techniques for PARAFAC modeling of urine metabolomic data. Metabolomics. 2016;12(12):1–13.

24. Li L, Hoefsloot H, de Graaf AA, Acar E, Smilde AK. Exploring dynamic metabolomics data with multiway data analysis: a simulation study. BMC Bioinformatics. 2022;23(31):1–22.

25. Twisk J, Bosman L, Hoekstra T, Rijnhart J, Welten M, Heymans M. Different ways to estimate treatment effects in randomised controlled trials. Contemporary Clinical Trials Communications. 2018;10:80–85.

26. Mattes RD. Oral fat exposure alters postprandial lipid metabolism in humans. The American Journal of Clinical Nutrition. 1996;63(6):911–917.

27. Wopereis S, Wolvers D, van Erk M, Gribnau M, Kremer B, van Dorsten FA, et al. Assessment of inflammatory resilience in healthy subjects using dietary lipid and glucose challenges. BMC Medical Genomics. 2013;6:44.

28. Kurata H. Virtual metabolic human dynamic model for pathological analysis and therapy design for diabetes. iScience. 2021;24(2):102101.

29. Bisgaard H. The Copenhagen Prospective Study on Asthma in Childhood (COPSAC): design, rationale, and baseline data from a longitudinal birth cohort study. Annals of Allergy, Asthma & Immunology. 2004;93(4):381–389.

30. Stroeve JH, van Wietmarschen H, Kremer BH, van Ommen B, Wopereis S. Phenotypic flexibility as a measure of health: the optimal nutritional stress response test. Genes & Nutrition. 2015;10(3):1–21.

31. Hitchcock FL. The Expression of a Tensor or a Polyadic as a Sum of Products. Journal of Mathematics and Physics. 1927;6(1):164–189.

32. Papalexakis EE, Faloutsos C, Sidiropoulos ND. Tensors for Data Mining and Data Fusion: Models, Applications, and Scalable Algorithms. ACM Trans Intell Syst Technol. 2016;8(2).

33. Acar E, Bingol CA, Bingol H, Bro R, Yener B. Multiway Analysis of Epilepsy Tensors. Bioinformatics. 2007;23(13):i10–i18.

34. Williams AH, Kim TH, Wang F, Vyas S, Ryu SI, Shenoy KV, et al. Unsupervised Discovery of Demixed, Low-Dimensional Neural Dynamics across Multiple Timescales through Tensor Component Analysis. Neuron. 2018;98(6):1099–1115.

35. Bro R. PARAFAC. Tutorial and applications. Chemometrics and Intelligent Laboratory Systems. 1997;38(2):149–171.

36. Tomasi G, Bro R. PARAFAC and missing values. Chemometrics and Intelligent Laboratory Systems. 2005;75(2):163–180.

37. Acar E, Dunlavy DM, Kolda TG, Mørup M. Scalable tensor factorizations for incomplete data. Chemometrics and Intelligent Laboratory Systems. 2011;106(1):41–56.

38. Håstad J. Tensor rank is NP-complete. Journal of Algorithms. 1990;11(4):644–654.

39. Adali T, Kantar F, Akhonda MABS, Strother S, Calhoun VD, Acar E. Reproducibility in Matrix and Tensor Decompositions: Focus on Model Match, Interpretability, and Uniqueness. IEEE Signal Processing Magazine. 2022;39(4):8–24.

40. Bro R, Kiers HA. A new efficient method for determining the number of components in PARAFAC models. Journal of Chemometrics. 2003;17(5):274–286.

41. Harshman RA, De Sarbo WS. An Application of PARAFAC to a Small Sample Problem, Demonstrating Preprocessing, Orthogonality Constraints, and Split-Half Diagnostic Techniques. In: Research Methods for Multimode Data Analysis. Praeger: New York; 1984. p. 602–642.

42. Bro R, Smilde AK. Centering and scaling in component analysis. Journal of Chemometrics. 2003;17(1):16–33.

43. Acar E, Dunlavy DM, Kolda TG. A scalable optimization approach for fitting canonical tensor decompositions. Journal of Chemometrics. 2011;25(2):67–86.

44. Bader BW, Kolda TG, et al.. Matlab Tensor Toolbox, Version 3.1;. https://www.tensortoolbox.org.

45. Kahler A, Zimmermann M, Langhans W. Suppression of hepatic fatty acid oxidation and food intake in men. Nutrition. 1999;15(11-12):819–828.

46. Saito K, Maekawa K, Pappan KL, Urata M, Ishikawa M, Kumagai Y, et al. Differences in metabolite profiles between blood matrices, ages, and sexes among Caucasian individuals and their inter-individual variations. Metabolomics. 2014;10(3):402–413.

47. Bays HE, Toth PP, Kris-Etherton PM, Abate N, Aronne LJ, Brown WV, et al. Obesity, adiposity, and dyslipidemia: A consensus statement from the National Lipid Association. Journal of Clinical Lipidology. 2013;7(4):304–383.

48. Lamon-Fava S, Wilson PWF, Schaefer EJ. Impact of Body Mass Index on Coronary Heart Disease Risk Factors in Men and Women. Arteriosclerosis, Thrombosis, and Vascular Biology. 1996;16:1509–1515.

49. Schmedes M, Balderas C, Aadland EK, Jacques H, Lavigne C, Graff IE, et al. The effect of lean-seafood and non-seafood diets on fasting and postprandial serum metabolites and lipid species: results from a randomized crossover intervention study in healthy adults. Nutrients. 2018;10(5):598.

50. Rivellese AA, Maffettone A, Vessby B, Uusitupa M, Hermansen K, Berglund L, et al. Effects of dietary saturated, monounsaturated and n-3 fatty acids on fasting lipoproteins, LDL size and post-prandial lipid metabolism in healthy subjects. Atherosclerosis. 2003;167(1):149–158.

51. Vilozni D, Bentur L, Efrati O, Barak A, Szeinberg A, Shoseyov D, et al. Exercise challenge test in 3-to 6-year-old asthmatic children. Chest. 2007;132(2):497–503.

52. Harshman RA. PARAFAC2: Mathematical and technical notes. UCLA working papers in phonetics. 1972;22:30–44.

53. Madsen KH, Churchill NW, Mørup M. Quantifying Functional Connectivity in Multi-Subject fMRI Data Using Component Models. Human Brain Mapping. 2017;38:882–899.

54. Roald M, Bhinge S, Jia C, Calhoun V, Adali T, Acar E. Tracing Network Evolution using the PARAFAC2 model. In: ICASSP'20; 2020. p. 1100–1104.

55. Acar E, Roald M, Hossain KM, Calhoun VD, Adali T. Tracing Evolving Networks using Tensor Factorizations vs. ICA-based Approaches. Frontiers in Neuroscience. 2022;16:861402.

56. Bro R, Andersson CA, Kiers HA. PARAFAC2—Part II. Modeling chromatographic data with retention time shifts. Journal of Chemometrics. 1999;13:295–309.